



ScanNet: Richly-annotated 3D Reconstructions of Indoor Scenes

Angela Dai¹ Angel X. Chang² Manolis Savva² Maciej Halber² Thomas Funkhouser² Matthias Nießner^{1,3}
¹Stanford University ²Princeton University ³Technical University of Munich

www.scan-net.org

Abstract

A key requirement for leveraging supervised deep learning methods is the availability of large, labeled datasets. Unfortunately, in the context of RGB-D scene understanding, very little data is available – current datasets cover a small range of scene views and have limited semantic annotations. To address this issue, we introduce ScanNet, an RGB-D video dataset containing 2.5M views in 1513 scenes annotated with 3D camera poses, surface reconstructions, and semantic segmentations. To collect this data, we designed an easy-to-use and scalable RGB-D capture system that includes automated surface reconstruction and crowd-sourced semantic annotation. We show that using this data helps achieve state-of-the-art performance on several 3D scene understanding tasks, including 3D object classification, semantic voxel labeling, and CAD model retrieval.

1. Introduction

Since the introduction of commodity RGB-D sensors, such as the Microsoft Kinect, the field of 3D geometry capture has gained significant attention and opened up a wide range of new applications. Although there has been significant effort on 3D reconstruction algorithms, general 3D scene understanding with RGB-D data has only very recently started to become popular. Research along semantic understanding is also heavily facilitated by the rapid progress of modern machine learning methods, such as neural models. One key to successfully applying these approaches is the availability of large, labeled datasets. While much effort has been made on 2D datasets [17, 44, 47], where images can be downloaded from the web and directly annotated, the situation for 3D data is more challenging. Thus, many of the current RGB-D datasets [74, 92, 77, 32] are orders of magnitude smaller than their 2D counterparts. Typically, 3D deep learning methods use synthetic data to mitigate this lack of real-world data [91, 6].

One of the reasons that current 3D datasets are small is because their capture requires much more effort, and effi-



Figure 1. Example reconstructed spaces in ScanNet annotated with instance-level object category labels through our crowdsourced annotation framework.

ciently providing (dense) annotations in 3D is non-trivial. Thus, existing work on 3D datasets often fall back to polygon or bounding box annotations on 2.5D RGB-D images [74, 92, 77], rather than directly annotating in 3D. In the latter case, labels are added manually by expert users (typically by the paper authors) [32, 71] which limits their overall size and scalability.

In this paper, we introduce ScanNet, a dataset of richly-annotated RGB-D scans of real-world environments containing 2.5M RGB-D images in 1513 scans acquired in 707 distinct spaces. The sheer magnitude of this dataset is larger than any other [58, 81, 92, 75, 3, 71, 32]. However, what makes it particularly valuable for research in scene understanding is its annotation with estimated calibration parameters, camera poses, 3D surface reconstructions, textured meshes, dense object-level semantic segmentations, and aligned CAD models (see Fig. 2). The semantic segmentations are more than an order of magnitude larger than any previous RGB-D dataset.

In the collection of this dataset, we have considered two main research questions: 1) how can we design a framework that allows many people to collect and annotate large

本文的主要工作

Dataset	Size	Labels	Annotation Tool	Reconstruction	CAD Models
NYU v2 [58]	464 scans	1449 frames	2D LabelMe-style [69]	none	some [25]
TUM [81]	47 scans	none	-	aligned poses (Vicon)	no
SUN 3D [92]	415 scans	8 scans	2D polygons	aligned poses [92]	no
SUN RGB-D [75]	10k frames	10k frames	2D polygons + bounding boxes	aligned poses [92]	no
BuildingParser [3]	265 rooms	265 rooms	CloudCompare [24]	point cloud	no
PiGraphs [71]	26 scans	26 scans	dense 3D, by the authors [71]	dense 3D [62]	no
SceneNN [32]	100 scans	100 scans	dense 3D, by the authors [60]	dense 3D [9]	no
ScanNet (ours)	1513 scans 2.5M frames	1513 scans	dense 3D, crowd-sourced MTurk labels also proj. to 2D frames	dense 3D [12]	yes

Table 1. Overview of RGB-D datasets for 3D reconstruction and semantic scene understanding. Note that in addition to the 1513 scans in ScanNet, we also provided dense 3D reconstruction and annotations on all NYU v2 sequences.

amounts of RGB-D data, and 2) can we use the rich annotations and data quantity provided in ScanNet to learn better 3D models for scene understanding?

To investigate the first question, we built a capture pipeline to help novices acquire semantically-labeled 3D models of scenes. A person uses an app on an iPad mounted with a depth camera to acquire RGB-D video, and then we process the data off-line and return a complete semantically-labeled 3D reconstruction of the scene. The challenges in developing such a framework are numerous, including how to perform 3D surface reconstruction robustly in a scalable pipeline and how to crowdsource semantic labeling. The paper discusses our study of these issues and documents our experience with scaling up RGB-D scan collection (20 people) and annotation (500 crowd workers).

To investigate the second question, we trained 3D deep networks with the data provided by ScanNet and tested their performance on several scene understanding tasks, including 3D object classification, semantic voxel labeling, and CAD model retrieval. For the semantic voxel labeling task, we introduce a new volumetric CNN architecture.

Overall, the contributions of this paper are:

- A large 3D dataset containing 1513 RGB-D scans of over 707 unique indoor environments with estimated camera parameters, surface reconstructions, textured meshes, semantic segmentations. We also provide CAD model placements for a subset of the scans.
- A design for efficient 3D data capture and annotation suitable for novice users.
- New RGB-D benchmarks and improved results for state-of-the-art machine learning methods on 3D object classification, semantic voxel labeling, and CAD model retrieval.
- A complete open source acquisition and annotation framework for dense RGB-D reconstructions.

2. Previous Work

A large number of RGB-D datasets have been captured and made publicly available for training and benchmarking [56, 34, 50, 65, 79, 83, 74, 4, 58, 81, 15, 55, 1, 68, 30, 51, 21,

48, 43, 92, 80, 61, 72, 93, 36, 16, 35, 57, 40, 29, 70, 52, 45, 95, 75, 9, 33, 85, 71, 32, 3, 10, 78, 2].¹ These datasets have been used to train models for many 3D scene understanding tasks, including semantic segmentation [67, 58, 26, 86], 3D object detection [73, 46, 27, 76, 77], 3D object classification [91, 53, 66], and others [94, 22, 23].

Most RGB-D datasets contain scans of individual objects. For example, the Redwood dataset [10] contains over 10,000 scans of objects annotated with class labels, 1,781 of which are reconstructed with KinectFusion [59]. Since the objects are scanned in isolation without scene context, the dataset's focus is mainly on evaluating surface reconstruction quality rather than semantic understanding of complete scenes.

One of the earliest and most popular datasets for RGB-D scene understanding is NYU v2 [74]. It is composed of 464 short RGB-D sequences, from which 1449 frames have been annotated with 2D polygons denoting semantic segmentations, as in LabelMe [69]. SUN RGB-D [75] follows up on this work by collecting 10,335 RGB-D frames annotated with polygons in 2D and bounding boxes in 3D. These datasets have scene diversity comparable to ours, but include only a limited range of viewpoints, and do not provide complete 3D surface reconstructions, dense 3D semantic segmentations, or a large set of CAD model alignments.

One of the first RGB-D datasets focused on long RGB-D sequences in indoor environments is SUN3D. It contains a set of 415 Kinect v1 sequences of 254 unique spaces. Although some objects were annotated manually with 2D polygons, and 8 scans have estimated camera poses based on user input, the bulk of the dataset does not include camera poses, 3D reconstructions, or semantic annotations.

Recently, Armeni et al. [3, 2] introduced an indoor dataset containing 3D meshes for 265 rooms captured with a custom Matterport camera and manually labeled with semantic annotations. The dataset is high-quality, but the cap-

¹A comprehensive and detailed overview of publicly-accessible RGB-D datasets is given by [20] at <http://www0.cs.ucl.ac.uk/staff/M.Firman/RGBDdatasets/>, which is updated on a regular basis.

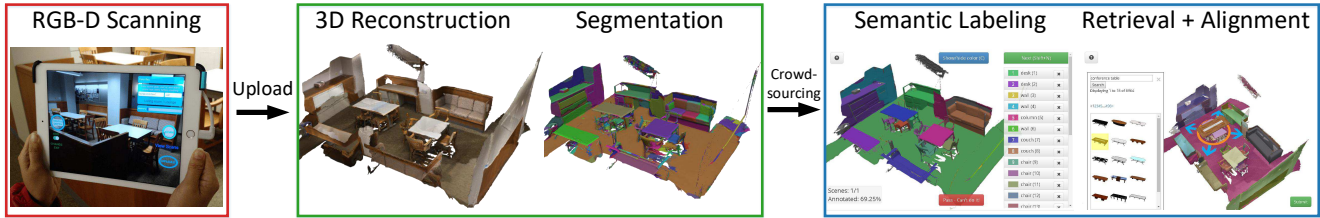


Figure 2. Overview of our RGB-D reconstruction and semantic annotation framework. **Left:** a novice user uses a handheld RGB-D device with our scanning interface to scan an environment. **Mid:** RGB-D sequences are uploaded to a processing server which produces 3D surface mesh reconstructions and their surface segmentations. **Right:** Semantic annotation tasks are issued for crowdsourcing to obtain instance-level object category annotations and 3D CAD model alignments to the reconstruction.

ture pipeline is based on expensive and less portable hardware. Furthermore, only a fused point cloud is provided as output. Due to the lack of raw color and depth data, its applicability to research on reconstruction and scene understanding from raw RGB-D input is limited.

The datasets most similar to ours are SceneNN [32] and PiGraphs [71], which are composed of 100 and 26 densely reconstructed and labeled scenes respectively. The annotations are done directly in 3D [60, 71]. However, both scanning and labeling are performed only by expert users (i.e. the authors), limiting the scalability of the system and the size of the dataset. In contrast, we design our RGB-D acquisition framework specifically for ease-of-use by untrained users and for scalable processing through crowdsourcing. This allows us to acquire a significantly larger dataset with more annotations (currently, 1513 sequences are reconstructed and labeled).

3. Dataset Acquisition Framework

In this section, we focus on the design of the framework used to acquire the ScanNet dataset (Fig. 2). We discuss design trade-offs in building the framework and relay findings on which methods were found to work best for large-scale RGB-D data collection and processing.

Our main goal driving the design of our framework was to allow untrained users to capture semantically labeled surfaces of indoor scenes with commodity hardware. Thus the RGB-D scanning system must be trivial to use, the data processing robust and automatic, the semantic annotations crowdsourced, and the flow of data through the system handled by a tracking server.

3.1. RGB-D Scanning

Hardware. There is a spectrum of choices for RGB-D sensor hardware. Our requirement for deployment to large groups of inexperienced users necessitates a portable and low-cost RGB-D sensor setup. We use the Structure sensor [63], a commodity RGB-D sensor with design similar to the Microsoft Kinect v1. We attach this sensor to a handheld device such as an iPhone or iPad (see Fig. 2 left) — results in this paper were collected using iPad Air2 devices. The

iPad RGB camera data is temporally synchronized with the depth sensor via hardware, providing synchronized depth and color capture at 30 Hz. Depth frames are captured at a resolution of 640×480 and color at 1296×968 pixels. We enable auto-white balance and auto-exposure by default.

Calibration. Our use of commodity RGB-D sensors necessitates unwarping of depth data and alignment of depth and color data. Prior work has focused mostly on controlled lab conditions with more accurate equipment to inform calibration for commodity sensors (e.g., Wang et al. [87]). However, this is not practical for novice users. Thus the user only needs to print out a checkerboard pattern, place it on a large, flat surface, and capture an RGB-D sequence viewing the surface from close to far away. This sequence, as well as a set of infrared and color frame pairs viewing the checkerboard, are uploaded by the user as input to the calibration. Our system then runs a calibration procedure based on [84, 14] to obtain intrinsic parameters for both depth and color sensors, and an extrinsic transformation of depth to color. We find that this calibration procedure is easy for users and results in improved data and consequently enhanced reconstruction quality.

User Interface. To make the capture process simple for untrained users, we designed an iOS app with a simple live RGB-D video capture UI (see Fig. 2 left). The user provides a name and scene type for the current scan and proceeds to record a sequence. During scanning, a log-scale RGB feature detector point metric is shown as a “featurefulness” bar to provide a rough measure of tracking robustness and reconstruction quality in different regions being scanned. This feature was critical for providing intuition to users who are not familiar with the constraints and limitations of 3D reconstruction algorithms.

Storage. We store scans as compressed RGB-D data on the device flash memory so that a stable internet connection is not required during scanning. The user can upload scans to the processing server when convenient by pressing an “upload” button. Our sensor units used 128 GB iPad Air2 devices, allowing for several hours of recorded RGB-D video. In practice, the bottleneck was battery life rather

than storage space. Depth is recorded as 16-bit unsigned short values and stored using standard zlib compression. RGB data is encoded with the H.264 codec with a high bitrate of 15 Mbps to prevent encoding artifacts. In addition to the RGB-D frames, we also record Inertial Measurement Unit (IMU) data, including acceleration, and angular velocities, from the Apple SDK. Timestamps are recorded for IMU, color, and depth images.

3.2. Surface Reconstruction

Once data has been uploaded from the iPad to our server, the first processing step is to estimate a densely-reconstructed 3D surface mesh and 6-DoF camera poses for all RGB-D frames. To conform with the goal for an automated and scalable framework, we choose methods that favor robustness and processing speed such that uploaded recordings can be processed at near real-time rates with little supervision.

Dense Reconstruction. We use volumetric fusion [11] to perform the dense reconstruction, since this approach is widely used in the context of commodity RGB-D data. There is a large variety of algorithms targeting this scenario [59, 88, 7, 62, 37, 89, 42, 9, 90, 38, 12]. We chose the BundleFusion system [12] as it was designed and evaluated for similar sensor setups as ours, and provides real-time speed while being reasonably robust given handheld RGB-D video data.

For each input scan, we first run BundleFusion [12] at a voxel resolution of 1 cm^3 . BundleFusion produces accurate pose alignments which we then use to perform volumetric integration through VoxelHashing [62] and extract a high resolution surface mesh using the Marching Cubes algorithm on the implicit TSDF (4 mm^3 voxels). The mesh is then automatically cleaned up with a set of filtering steps to merge close vertices, delete duplicate and isolated mesh parts, and finally to downsample the mesh to high, medium, and low resolution versions (each level reducing the number of faces by a factor of two).

Orientation. After the surface mesh is extracted, we automatically align it and all camera poses to a common coordinate frame with the z -axis as the up vector, and the xy plane aligned with the floor plane. To perform this alignment, we first extract all planar regions of sufficient size, merge regions defined by the same plane, and sort them by normal (we use a normal threshold of 25° and a planar offset threshold of 5 cm). We then determine a prior for the up vector by projecting the IMU gravity vectors of all frames into the coordinates of the first frame. This allows us to select the floor plane based on the scan bounding box and the normal most similar to the IMU up vector direction. Finally, we use a PCA on the mesh vertices to determine the rotation around the z -axis and translate the scan such that its bounds are within the positive octant of the coordinate system.

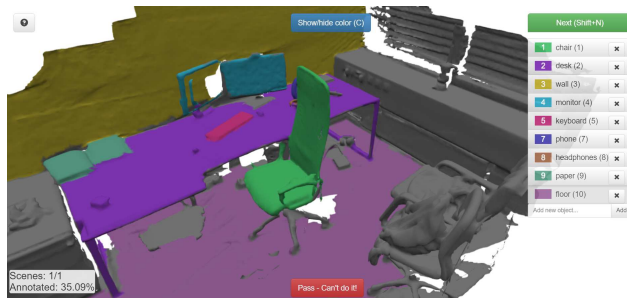


Figure 3. Our web-based crowdsourcing interface for annotating a scene with instance-level object category labels. The right panel lists object instances already annotated in the scene with matching painted colors. This annotation is in progress at $\approx 35\%$, with gray regions indicating unannotated surfaces.

Validation. This reconstruction process is automatically triggered when a scan is uploaded to the processing server and runs unsupervised. In order to establish a clean snapshot to construct the ScanNet dataset reported in this paper, we automatically discard scan sequences that are short, have high residual reconstruction error, or have low percentage of aligned frames. We then manually check for and discard reconstructions with noticeable misalignments.

3.3. Semantic Annotation

After a reconstruction is produced by the processing server, annotation HITs (Human Intelligence Tasks) are issued on the Amazon Mechanical Turk crowdsourcing market. The two HITs that we crowdsource are: i) instance-level object category labeling of all surfaces in the reconstruction, and ii) 3D CAD model alignment to the reconstruction. These annotations are crowdsourced using web-based interfaces to again maintain the overall scalability of the framework.

Instance-level Semantic Labeling. Our first annotation step is to obtain a set of object instance-level labels directly on each reconstructed 3D surface mesh. This is in contrast to much prior work that uses 2D polygon annotations on RGB or RGB-D images, or 3D bounding box annotations.

We developed a WebGL interface that takes as input the low-resolution surface mesh of a given reconstruction and a conservative over-segmentation of the mesh using a normal-based graph cut method [19, 39]. The crowd worker then selects segments to annotate with instance-level object category labels (see Fig. 3). Each worker is required to annotate at least 25% of the surfaces in a reconstruction, and encouraged to annotate more than 50% before submission. Each scan is annotated by multiple workers (scans in ScanNet are annotated by 2.3 workers on average).

A key challenge in designing this interface is to enable efficient annotation by workers who have no prior experience with the task, or 3D interfaces in general. Our interface uses a simple painting metaphor where clicking and drag-

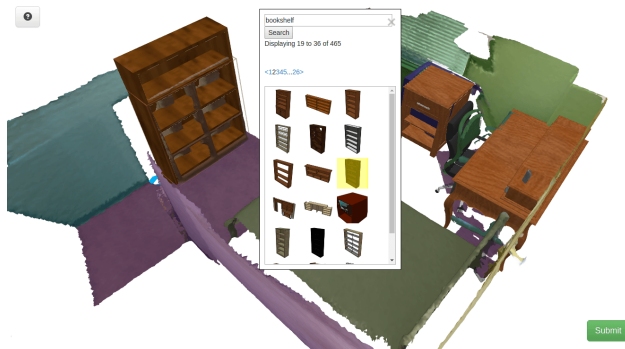


Figure 4. Crowdsourcing interface for aligning CAD models to objects in a reconstruction. Objects can be clicked to initiate an assisted search for CAD models (see list of bookshelves in middle). A suggested model is placed at the position of the clicked object, and the user then refines the position and orientation. A desk, chair, and nightstand have been already placed here.

ging over surfaces paints segments with a given label and corresponding color. This functions similarly to 2D painting and allows for erasing and modifying existing regions.

Another design requirement is to allow for freeform text labels, to reduce the inherent bias and scalability issues of pre-selected label lists. At the same time, it is desirable to guide users for consistency and coverage of basic object types. To achieve this, the interface provides autocomplete functionality over all labels previously provided by other workers that pass a frequency threshold (> 5 annotations). Workers are always allowed to add arbitrary text labels to ensure coverage and allow expansion of the label set.

Several additional design details are important to ensure usability by novice workers. First, a simple distance check for connectedness is used to disallow labeling of disconnected surfaces with the same label. Earlier experiments without this constraint resulted in two undesirable behaviors: cheating by painting many surfaces with a few labels, and labeling of multiple object instances with the same label. Second, the 3D nature of the data is challenging for novice users. Therefore, we first show a full turntable rotation of each reconstruction and instruct workers to change the view using a rotating turntable metaphor. Without the turntable rotation animation, many workers only annotated from the initial view and never used camera controls despite the provided instructions.

CAD Model Retrieval and Alignment. In the second annotation task, a crowd worker was given a reconstruction already annotated with object instances and asked to place appropriate 3D CAD models to represent major objects in the scene. The challenge of this task lies in the selection of closely matching 3D models from a large database, and in precisely aligning each model to the 3D position of the corresponding object in the reconstruction.

We implemented an assisted object retrieval interface

Statistic	SceneNN [32]	ScanNet
# of scans	100	1513
# of RGB-D frames	2,475,905	2,492,518
floor area (avg / sum m^2)	22.6 / 2,124	22.6 / 34,453
surface area (avg / sum m^2)	75.3 / 7,078	51.6 / 78,595
labeled objects (avg / sum)	15.8 / 1482	24.1 / 36,213

Table 2. Summary statistics for ScanNet compared to the most similar existing dataset (SceneNN [32]). ScanNet has an order of magnitude more scans, with 3D surface mesh reconstructions covering more than ten times the floor and surface area, and with more than 36,000 annotated object instances.

where clicking on a previously labeled object in a reconstruction immediately searched for CAD models with the same category label in the ShapeNetCore [6] dataset, and placed one example model such that it overlaps with the oriented bounding box of the clicked object (see Fig. 4). The worker then used keyboard and mouse-based controls to adjust the alignment of the model, and was allowed to submit the task once at least three CAD models were placed.

Using this interface, we collected sets of CAD models aligned to each ScanNet reconstruction. Preliminary results indicate that despite the challenging nature of this task, workers select semantically appropriate CAD models to match objects in the reconstructions. The main limitation of this interface is due to the mismatch between the corpus of available CAD models and the objects observed in the ScanNet scans. Despite the diversity of the ShapeNet CAD model dataset (55K objects), it is still hard to find exact instance-level matches for chairs, desks and more rare object categories. A promising way to alleviate this limitation is to algorithmically suggest candidate retrieved and aligned CAD models such that workers can perform an easier verification and adjustment task.

4. ScanNet Dataset

In this section, we summarize the data we collected using our framework to establish the ScanNet dataset. This dataset is a snapshot of available data from roughly one month of data acquisition by 20 users at locations in several countries. It has annotations by more than 500 crowd workers on the Mechanical Turk platform. Since the presented framework runs in an unsupervised fashion and people are continuously collecting data, this dataset continues to grow organically. Here, we report some statistics for an initial snapshot of 1513 scans, which are summarized in Table 2.

Fig. 5 plots the distribution of scanned scenes over different types of real-world spaces. ScanNet contains a variety of spaces such as offices, apartments, and bathrooms. The dataset contains a diverse set of spaces ranging from small (e.g., bathrooms, closets, utility rooms) to large (e.g., apartments, classrooms, and libraries). Each scan has been annotated with instance-level semantic category labels through

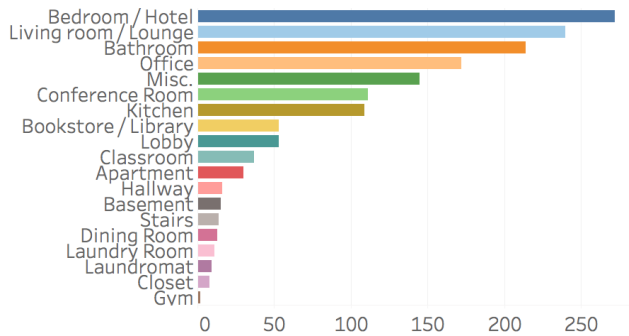


Figure 5. Distribution of the scans in ScanNet organized by type.

our crowdsourcing task. In total, we deployed 3,391 annotation tasks to annotate all 1513 scans.

The text labels used by crowd workers to annotate object instances are all mapped to the object category sets of NYU v2 [58], ModelNet [91], ShapeNet [6], and WordNet [18] synsets. This mapping is made more robust by a preprocess that collapses the initial text labels through synonym and misspelling detection.

In addition to reconstructing and annotating the 1513 ScanNet scans, we have processed all the NYU v2 RGB-D sequences with our framework. The result is a set of dense reconstructions of the NYU v2 spaces with instance-level object annotations in 3D that are complementary in nature to the existing image-based annotations.

We also deployed the CAD model alignment crowdsourcing task to collect a total of 107 virtual scene interpretations consisting of aligned ShapeNet models placed on a subset of 52 ScanNet scans by 106 workers. There were a total of 681 CAD model instances (of 296 unique models) retrieved and placed on the reconstructions, with an average of 6.4 CAD model instances per annotated scan.

For more detailed statistics on this first ScanNet dataset snapshot, please see the supplemental material.

5. Tasks and Benchmarks

In this section, we describe the three tasks we developed as benchmarks for demonstrating the value of ScanNet data.

Train/Test split statistics. Table 3 shows the test and training splits of ScanNet in the context of the object classification and dense voxel prediction benchmarks. Note that our data is significantly larger than any existing comparable dataset. We use these tasks to demonstrate that ScanNet enables the use of deep learning methods for 3D scene understanding tasks with supervised training, and compare performance to that using data from other existing datasets.

5.1. 3D Object Classification

With the availability of large-scale synthetic 3D datasets such as [91, 6] and recent advances in 3D deep learn-

		Scans		Instances	
		#Train	#Test	#Train	#Test
Object Classification	ScanNet	1205	312	9305	2606
	NYU	452	80	3260	613
	SceneNN	70	12	377	66
Semantic Voxel Labeling	ScanNet	1201	312	80554	21300

Table 3. Train/Test split for object classification and dense voxel prediction tasks. Note that the number of instances does not include the rotation augmentation.

ing, research has developed approaches to classify objects using only geometric data with volumetric deep nets [91, 82, 52, 13, 66]. All of these methods train on purely synthetic data and focus on isolated objects. Although they show limited evaluation on real-world data, a larger evaluation on realistic scanning data is largely missing. When training data is synthetic and test is performed on real data, there is also a significant discrepancy of test performance, as data characteristics, such as noise and occlusions patterns, are inherently different.

With ScanNet, we close this gap as we have captured a sufficiently large amount of 3D data to use real-world RGB-D input for both training and test sets. For this task, we use the bounding boxes of annotated objects in ScanNet, and isolate the contained geometry. As a result, we obtain local volumes around each object instance for which we know the annotated category. The goal of the task is to classify the object represented by a set of scanned points within a given bounding box. For this benchmark, we use 17 categories, with 9,677 train instances and 2,606 test instances.

Network and training. For object classification, we follow the network architecture of the 3D Network-in-Network of [66], without the multi-orientation pooling step. In order to classify partial data, we add a second channel to the 30^3 occupancy grid input, indicating known and unknown regions (with 1 and 0, respectively) according to the camera scanning trajectory. As in Qi et al. [66], we use an SGD solver with learning rate 0.01 and momentum 0.9, decaying the learning rate by half every 20 epochs, and training the model for 200 epochs. We augment training samples with 12 instances of different rotations (including both elevation and tilt), resulting in a total training set of 111,660 samples.

Benchmark performance. As a baseline evaluation, we run the 3D CNN approach of Qi et al. [66]. Table 4 shows the performance of 3D shape classification with different train and test sets. The first two columns show results on synthetic test data from ShapeNet [6] including both complete and partial data. Naturally, training with the corresponding synthetic counterparts of ShapeNet provides the best performance, as data characteristics are shared. However, the more interesting case is real-world test data (right-

most two columns); here, we show results on test sets of SceneNN [32] and ScanNet. First, we see that training on synthetic data allows only for limited knowledge transfer (first two rows). Second, although the relatively small SceneNN dataset is able to learn within its own dataset to a reasonable degree, it does not generalize to the larger variety of environments found in ScanNet. On the other hand, training on ScanNet translates well to testing on SceneNN; as a result, the test results on SceneNN are significantly improved by using the training data from ScanNet. Interestingly enough, these results can be slightly improved when mixing training data of ScanNet with partial scans of ShapeNet (last row).

Training Set	Synthetic Test Sets		Real Test Sets	
	ShapeNet	ShapeNet Partial	SceneNN	ScanNet
ShapeNet	92.5	37.6	68.2	39.5
ShapeNet Partial	88.5	92.1	72.7	45.7
SceneNN	19.9	27.7	69.8	48.2
NYU	26.2	26.6	72.7	53.2
ScanNet	21.4	31.0	78.8	74.9
ScanNet +ShapeNet Par.	79.7	89.8	81.2	76.6

Table 4. 3D object classification benchmark performance. Percentages give the classification accuracy over all models in each test set (average instance accuracy).

5.2. Semantic Voxel Labeling

A common task on RGB data is semantic segmentation (i.e. labeling pixels with semantic classes) [49]. With our data, we can extend this task to 3D, where the goal is to predict the semantic object label on a per-voxel basis. This task of predicting a semantic class for each visible 3D voxel has been addressed by some prior work, but using hand-crafted features to predict a small number of classes [41, 86], or focusing on outdoor environments [8, 5].

Data Generation. We first voxelize a scene and obtain a dense voxel grid with 2cm^3 voxels, where every voxel stores its TSDF value and object class annotation (empty space and unlabeled surface points have their own respective classes). We now extract subvolumes of the scene volume, of dimension $2 \times 31 \times 31 \times 62$ and spatial extent $1.5\text{m} \times 1.5\text{m} \times 3\text{m}$; i.e., a voxel size of $\approx 4.8\text{cm}^3$; the two channels represent the occupancy and known/unknown space according to the camera trajectory. These sample volumes are aligned with the xy -ground plane. For ground truth data generation, voxel labels are propagated from the scene voxelization to these sample volumes. The samples are chosen that $\geq 2\%$ of the voxels are occupied (i.e., on the surface), and $\geq 70\%$ of these surface voxels have valid annotations; samples not meeting these criteria are discarded. Across ScanNet, we generate 93,721 subvolume examples for training, augmented by 8 rotations each (i.e., 749,768

training samples), from 1201 training scenes. In addition, we extract 18,750 sample volumes for testing, which are also augmented by 8 rotations each (i.e., 150,000 test samples) from 312 test scenes. We have 20 object class labels plus 1 class for free space.

Network and training. For the semantic voxel labeling task, we propose a network which predicts class labels for a column of voxels in a scene according to the occupancy characteristics of the voxels’ neighborhood. In order to infer labels for an entire scene, we use the network to predict a label for every voxel column at test time (i.e., every xy position that has voxels on the surface). The network takes as input a $2 \times 31 \times 31 \times 62$ volume and uses a series of fully convolutional layers to simultaneously predict class scores for the center column of 62 voxels. We use ReLU and batch normalization for all layers (except the last) in the network. To account for the unbalanced training data over the class labels, we weight the cross entropy loss with the inverse log of the histogram of the train data.

We use an SGD solver with learning rate 0.01 and momentum 0.9, decaying the learning rate by half every 20 epochs, and train the model for 100 epochs.

Quantitative Results. The goal of this task is to predict semantic labels for all visible surface voxels in a given 3D scene; i.e., every voxel on a visible surface receives one of the 20 object class labels. We use NYU2 labels, and list voxel classification results on ScanNet in Table 7. We achieve an voxel classification accuracy of 73.0% over the set of 312 test scenes, which is based purely on the geometric input (no color is used).

In Table 5, we show our semantic voxel labeling results on the NYU2 dataset [58]. We are able to outperform previous methods which are trained on limited sets of real-world data using our volumetric classification network. For instance, Hermans et al. [31] classify RGB-D frames using a dense random decision forest in combination with a conditional random field. Additionally, SemanticFusion [54] uses a deep net trained on RGB-D frames, and regularize the predictions with a CRF over a 3D reconstruction of the frames; note that we compare to their classification results before the CRF regularization. SceneNet trains on a large synthetic dataset and fine-tunes on NYU2. Note that in contrast to Hermans et al. and SemanticFusion, neither we nor SceneNet use RGB information.

Note that we do not explicitly enforce prediction consistency between neighboring voxel columns when the test volume is slid across the xy plane. This could be achieved with a volumetric CRF [64], as used in [86]; however, our goal in this task to focus exclusively on the per-voxel classification accuracy.

	floor	wall	chair	table	window	bed	sofa	tv	objs.	furn.	ceil.	avg.
Hermans et al. [31]	91.5	71.8	41.9	27.7	46.1	68.4	28.5	38.4	8.6	37.1	83.4	49.4
SemanticFusion [54]*	92.6	86.0	58.4	34.0	60.5	61.7	47.3	33.9	59.1	63.7	43.4	58.2
SceneNet [28]	96.2	85.3	61.0	43.8	30.0	72.5	62.8	19.4	50.0	60.4	74.1	59.6
Ours (ScanNet + NYU)	99.0	55.8	67.6	50.9	63.1	81.4	67.2	35.8	34.6	65.6	46.2	60.7

Table 5. Dense pixel classification accuracy on NYU2 [58]. Note that both SemanticFusion [54] and Hermans et. al. [31] use both geometry and color, and that Hermans et al. uses a CRF, unlike our approach which is *geometry-only* and has only unary predictions. The reported SemanticFusion classification is on the 13 class task (13 class average accuracy of 58.9%).

Train	Retrieval from ShapeNet	
	Top 1 NN	Top 3 NNs
ShapeNet	10.4%	8.0%
ScanNet	12.7%	11.7%
ShapeNet + ScanNet	77.5%	77.0%

Table 6. 3D model retrieval benchmark performance. Nearest neighbor models are retrieved for ScanNet objects from ShapeNet-Core. Percentages indicate average instance accuracy of retrieved model to query region.

Class	% of Test Scenes	Accuracy
Floor	35.7%	90.3%
Wall	38.8%	70.1%
Chair	3.8%	69.3%
Sofa	2.5%	75.7%
Table	3.3%	68.4%
Door	2.2%	48.9%
Cabinet	2.4%	49.8%
Bed	2.0%	62.4%
Desk	1.7%	36.8%
Toilet	0.2%	69.9%
Sink	0.2%	39.4%
Window	0.4%	20.1%
Picture	0.2%	3.4%
Bookshelf	1.6%	64.6%
Curtain	0.7%	7.0%
Shower Curtain	0.04%	46.8%
Counter	0.6%	32.1%
Refrigerator	0.3%	66.4%
Bathtub	0.2%	74.3%
OtherFurniture	2.9%	19.5%
Total	-	73.0%

Table 7. Semantic voxel label prediction accuracy on ScanNet test scenes.

5.3. 3D Object Retrieval

Another important task is retrieval of similar CAD models given (potentially partial) RGB-D scans. To this end, one wants to learn a shape embedding where a feature descriptor defines geometric similarity between shapes. The core idea is to train a network on a shape classification task where a shape embedding can be learned as byproduct of the classification task. For instance, Wu et al. [91] and Qi et al. [66] use this technique to perform shape retrieval queries within the ShapeNet database.

With ScanNet, we have established category-level correspondences between real-world objects and ShapeNet models. This allows us to train on a classification problem where both real and synthetic data are mixed inside of each category using real and synthetic data within shared class labels.

Thus, we can learn an embedding between real and synthetic data in order to perform model retrieval for RGB-D scans. To this end, we use the volumetric shape classification network by Qi et al. [66], we use the same training procedure as in Sec. 5.1. Nearest neighbors are retrieved based on the ℓ_2 distance between the extracted feature descriptors, and measured against the ground truth provided by the CAD model retrieval task. In Table 6, we show object retrieval results using objects from ScanNet to query for nearest neighbor models from ShapeNetCore. Note that training on ShapeNet and ScanNet independently results in poor retrieval performance, as neither are able to bridge the gap between the differing characteristics of synthetic and real-world data. Training on both ShapeNet and ScanNet together is able to find an embedding of shape similarities between both data modalities, resulting in much higher retrieval accuracy.

6. Conclusion

This paper introduces ScanNet: a large-scale RGB-D dataset of 1513 scans with surface reconstructions, instance-level object category annotations, and 3D CAD model placements. To make the collection of this data possible, we designed a scalable RGB-D acquisition and semantic annotation framework that we provide for the benefit of the community. We demonstrated that the richly-annotated scan data collected so far in ScanNet is useful in achieving state-of-the-art performance on several 3D scene understanding tasks; we hope that ScanNet will inspire future work on many other tasks.

Acknowledgments

This project is funded by Google Tango, Intel, NSF (IIS-1251217 and VEC 1539014/1539099), and a Stanford Graduate fellowship. We also thank Occipital for donating structure sensors and Nvidia for hardware donations, as well as support by the Max-Planck Center for Visual Computing and the Stanford CURIS program. Further, we thank Toan Vuong, Joseph Chang, and Helen Jiang for help on the mobile scanning app and the scanning process, and Hope Casey-Allen and Duc Nguyen for early prototypes of the annotation interfaces. Last but not least, we would like to thank all the volunteers who helped with scanning and getting us access to scanning spaces.

References

- [1] A. Aldoma, F. Tombari, L. Di Stefano, and M. Vincze. A global hypotheses verification method for 3D object recognition. In *European Conference on Computer Vision*, pages 511–524. Springer, 2012. [2](#)
- [2] I. Armeni, S. Sax, A. R. Zamir, and S. Savarese. Joint 2d-3d-semantic data for indoor scene understanding. *arXiv preprint arXiv:1702.01105*, 2017. [2](#)
- [3] I. Armeni, O. Sener, A. R. Zamir, H. Jiang, I. Brilakis, M. Fischer, and S. Savarese. 3D semantic parsing of large-scale indoor spaces. *CVPR*, 2016. [1](#), [2](#)
- [4] I. B. Barbosa, M. Cristani, A. Del Bue, L. Bazzani, and V. Murino. Re-identification with RGB-D sensors. In *European Conference on Computer Vision*, pages 433–442. Springer, 2012. [2](#)
- [5] M. Blaha, C. Vogel, A. Richard, J. D. Wegner, T. Pock, and K. Schindler. Large-scale semantic 3d reconstruction: an adaptive multi-resolution model for multi-class volumetric labeling. In *Proceedings of the IEEE Conference on Computer Vision and Pattern Recognition*, pages 3176–3184, 2016. [7](#)
- [6] A. X. Chang, T. Funkhouser, L. Guibas, P. Hanrahan, Q. Huang, Z. Li, S. Savarese, M. Savva, S. Song, H. Su, et al. ShapeNet: An information-rich 3D model repository. *arXiv preprint arXiv:1512.03012*, 2015. [1](#), [5](#), [6](#)
- [7] J. Chen, D. Bautembach, and S. Izadi. Scalable real-time volumetric surface reconstruction. *ACM Transactions on Graphics (TOG)*, 32(4):113, 2013. [4](#)
- [8] I. Cherabier, C. Häne, M. R. Oswald, and M. Pollefeys. Multi-label semantic 3d reconstruction using voxel blocks. In *3D Vision (3DV), 2016 Fourth International Conference on*, pages 601–610. IEEE, 2016. [7](#)
- [9] S. Choi, Q.-Y. Zhou, and V. Koltun. Robust reconstruction of indoor scenes. In *2015 IEEE Conference on Computer Vision and Pattern Recognition (CVPR)*, pages 5556–5565. IEEE, 2015. [2](#), [4](#)
- [10] S. Choi, Q.-Y. Zhou, S. Miller, and V. Koltun. A large dataset of object scans. *arXiv:1602.02481*, 2016. [2](#)
- [11] B. Curless and M. Levoy. A volumetric method for building complex models from range images. In *Proceedings of the 23rd annual conference on Computer graphics and interactive techniques*, pages 303–312. ACM, 1996. [4](#)
- [12] A. Dai, M. Nießner, M. Zollöfer, S. Izadi, and C. Theobalt. BundleFusion: Real-time globally consistent 3D reconstruction using on-the-fly surface re-integration. *arXiv preprint arXiv:1604.01093*, 2016. [2](#), [4](#)
- [13] A. Dai, C. R. Qi, and M. Nießner. Shape completion using 3d-encoder-predictor cnns and shape synthesis. *arXiv preprint arXiv:1612.00101*, 2016. [6](#)
- [14] M. Di Cicco, L. Iocchi, and G. Grisetti. Non-parametric calibration for depth sensors. *Robotics and Autonomous Systems*, 74:309–317, 2015. [3](#)
- [15] F. Endres, J. Hess, N. Engelhard, J. Sturm, D. Cremers, and W. Burgard. An evaluation of the RGB-D SLAM system. In *Robotics and Automation (ICRA), 2012 IEEE International Conference on*, pages 1691–1696. IEEE, 2012. [2](#)
- [16] N. Erdogmus and S. Marcel. Spoofing in 2D face recognition with 3D masks and anti-spoofing with Kinect. In *Biometrics: Theory, Applications and Systems (BTAS), 2013 IEEE Sixth International Conference on*, pages 1–6. IEEE, 2013. [2](#)
- [17] M. Everingham, L. Van Gool, C. K. Williams, J. Winn, and A. Zisserman. The PASCAL visual object classes (VOC) challenge. *International journal of computer vision*, 88(2):303–338, 2010. [1](#)
- [18] C. Fellbaum. *WordNet*. Wiley Online Library, 1998. [6](#)
- [19] P. F. Felzenszwalb and D. P. Huttenlocher. Efficient graph-based image segmentation. *International Journal of Computer Vision*, 59(2):167–181, 2004. [4](#)
- [20] M. Firman. RGBD datasets: Past, present and future. In *CVPR Workshop on Large Scale 3D Data: Acquisition, Modeling and Analysis*, 2016. [2](#)
- [21] S. Fothergill, H. Mentis, P. Kohli, and S. Nowozin. Instructing people for training gestural interactive systems. In *Proceedings of the SIGCHI Conference on Human Factors in Computing Systems*, pages 1737–1746. ACM, 2012. [2](#)
- [22] D. F. Fouhey, A. Gupta, and M. Hebert. Data-driven 3D primitives for single image understanding. In *Proceedings of the IEEE International Conference on Computer Vision*, pages 3392–3399, 2013. [2](#)
- [23] D. F. Fouhey, A. Gupta, and M. Hebert. Unfolding an indoor origami world. In *European Conference on Computer Vision*, pages 687–702. Springer, 2014. [2](#)
- [24] D. Girardeau-Montaut. CloudCompare3D point cloud and mesh processing software. *OpenSource Project*, 2011. [2](#)
- [25] R. Guo and D. Hoiem. Support surface prediction in indoor scenes. In *Proceedings of the IEEE International Conference on Computer Vision*, pages 2144–2151, 2013. [2](#)
- [26] S. Gupta, P. Arbelaez, and J. Malik. Perceptual organization and recognition of indoor scenes from RGB-D images. In *Proceedings of the IEEE Conference on Computer Vision and Pattern Recognition*, pages 564–571, 2013. [2](#)
- [27] S. Gupta, R. Girshick, P. Arbeláez, and J. Malik. Learning rich features from RGB-D images for object detection and segmentation. In *European Conference on Computer Vision*, pages 345–360. Springer, 2014. [2](#)
- [28] A. Handa, V. Patraucean, V. Badrinarayanan, S. Stent, and R. Cipolla. Scenenet: Understanding real world indoor scenes with synthetic data. *arXiv preprint arXiv:1511.07041*, 2015. [8](#)
- [29] A. Handa, T. Whelan, J. McDonald, and A. J. Davison. A benchmark for RGB-D visual odometry, 3D reconstruction and SLAM. In *2014 IEEE International Conference on Robotics and Automation (ICRA)*, pages 1524–1531. IEEE, 2014. [2](#)
- [30] V. Hedau, D. Hoiem, and D. Forsyth. Recovering free space of indoor scenes from a single image. In *Computer Vision and Pattern Recognition (CVPR), 2012 IEEE Conference on*, pages 2807–2814. IEEE, 2012. [2](#)
- [31] A. Hermans, G. Floros, and B. Leibe. Dense 3D semantic mapping of indoor scenes from RGB-D images. In *Robotics and Automation (ICRA), 2014 IEEE International Conference on*, pages 2631–2638. IEEE, 2014. [7](#), [8](#)

- [32] B.-S. Hua, Q.-H. Pham, D. T. Nguyen, M.-K. Tran, L.-F. Yu, and S.-K. Yeung. SceneNN: A scene meshes dataset with annotations. In *International Conference on 3D Vision (3DV)*, volume 1, 2016. 1, 2, 3, 5, 7
- [33] M. Innmann, M. Zollhöfer, M. Nießner, C. Theobalt, and M. Stamminger. VolumeDeform: Real-time volumetric non-rigid reconstruction. *arXiv preprint arXiv:1603.08161*, 2016. 2
- [34] C. Ionescu, F. Li, and C. Sminchisescu. Latent structured models for human pose estimation. In *2011 International Conference on Computer Vision*, pages 2220–2227. IEEE, 2011. 2
- [35] C. Ionescu, D. Papava, V. Olaru, and C. Sminchisescu. Human3.6M: Large scale datasets and predictive methods for 3D human sensing in natural environments. *IEEE transactions on pattern analysis and machine intelligence*, 36(7):1325–1339, 2014. 2
- [36] A. Janoch, S. Karayev, Y. Jia, J. T. Barron, M. Fritz, K. Saenko, and T. Darrell. A category-level 3D object dataset: Putting the Kinect to work. In *Consumer Depth Cameras for Computer Vision*, pages 141–165. Springer, 2013. 2
- [37] O. Kähler, V. Adrian Prisacariu, C. Yuheng Ren, X. Sun, P. Torr, and D. Murray. Very high frame rate volumetric integration of depth images on mobile devices. *IEEE Transactions on Visualization and Computer Graphics*, 21(11):1241–1250, 2015. 4
- [38] O. Kähler, V. A. Prisacariu, and D. W. Murray. Real-time large-scale dense 3D reconstruction with loop closure. In *European Conference on Computer Vision*, pages 500–516. Springer, 2016. 4
- [39] A. Karpathy, S. Miller, and L. Fei-Fei. Object discovery in 3D scenes via shape analysis. In *Robotics and Automation (ICRA), 2013 IEEE International Conference on*, pages 2088–2095. IEEE, 2013. 4
- [40] M. Kepski and B. Kwolek. Fall detection using ceiling-mounted 3D depth camera. In *Computer Vision Theory and Applications (VISAPP), 2014 International Conference on*, volume 2, pages 640–647. IEEE, 2014. 2
- [41] B.-s. Kim, P. Kohli, and S. Savarese. 3d scene understanding by voxel-crf. In *Proceedings of the IEEE International Conference on Computer Vision*, pages 1425–1432, 2013. 7
- [42] M. Klingensmith, I. Dryanovski, S. Srinivasa, and J. Xiao. Chisel: Real time large scale 3D reconstruction onboard a mobile device using spatially hashed signed distance fields. In *Robotics: Science and Systems*, 2015. 4
- [43] H. S. Koppula, R. Gupta, and A. Saxena. Learning human activities and object affordances from RGB-D videos. *The International Journal of Robotics Research*, 32(8):951–970, 2013. 2
- [44] A. Krizhevsky, I. Sutskever, and G. E. Hinton. ImageNet classification with deep convolutional neural networks. In *Advances in neural information processing systems*, pages 1097–1105, 2012. 1
- [45] Y. Li, A. Dai, L. Guibas, and M. Nießner. Database-assisted object retrieval for real-time 3D reconstruction. In *Computer Graphics Forum*, volume 34, pages 435–446. Wiley Online Library, 2015. 2
- [46] D. Lin, S. Fidler, and R. Urtasun. Holistic scene understanding for 3D object detection with RGBD cameras. In *Proceedings of the IEEE International Conference on Computer Vision*, pages 1417–1424, 2013. 2
- [47] T.-Y. Lin, M. Maire, S. Belongie, J. Hays, P. Perona, D. Ramanan, P. Dollár, and C. L. Zitnick. Microsoft COCO: Common objects in context. In *European Conference on Computer Vision*, pages 740–755. Springer, 2014. 1
- [48] L. Liu and L. Shao. Learning discriminative representations from RGB-D video data. In *IJCAI*, volume 1, page 3, 2013. 2
- [49] J. Long, E. Shelhamer, and T. Darrell. Fully convolutional networks for semantic segmentation. In *Proceedings of the IEEE Conference on Computer Vision and Pattern Recognition*, pages 3431–3440, 2015. 7
- [50] M. Luber, L. Spinello, and K. O. Arras. People tracking in RGB-D data with on-line boosted target models. In *2011 IEEE/RSJ International Conference on Intelligent Robots and Systems*, pages 3844–3849. IEEE, 2011. 2
- [51] J. Mason, B. Marthi, and R. Parr. Object disappearance for object discovery. In *2012 IEEE/RSJ International Conference on Intelligent Robots and Systems*, pages 2836–2843. IEEE, 2012. 2
- [52] O. Mattausch, D. Panozzo, C. Mura, O. Sorkine-Hornung, and R. Pajarola. Object detection and classification from large-scale cluttered indoor scans. In *Computer Graphics Forum*, volume 33, pages 11–21. Wiley Online Library, 2014. 2, 6
- [53] D. Maturana and S. Scherer. VoxNet: A 3D convolutional neural network for real-time object recognition. In *Intelligent Robots and Systems (IROS), 2015 IEEE/RSJ International Conference on*, pages 922–928. IEEE, 2015. 2
- [54] J. McCormac, A. Handa, A. Davison, and S. Leutenegger. Semanticfusion: Dense 3d semantic mapping with convolutional neural networks. *arXiv preprint arXiv:1609.05130*, 2016. 7, 8
- [55] S. Meister, S. Izadi, P. Kohli, M. Hämmerle, C. Rother, and D. Kondermann. When can we use KinectFusion for ground truth acquisition. In *Workshop on Color-Depth Camera Fusion in Robotics, IROS*, volume 2, 2012. 2
- [56] A. Mian, M. Bennamoun, and R. Owens. On the repeatability and quality of keypoints for local feature-based 3D object retrieval from cluttered scenes. *International Journal of Computer Vision*, 89(2-3):348–361, 2010. 2
- [57] R. Min, N. Kose, and J.-L. Dugelay. KinectFaceDB: A Kinect database for face recognition. *IEEE Transactions on Systems, Man, and Cybernetics: Systems*, 44(11):1534–1548, 2014. 2
- [58] P. K. Nathan Silberman, Derek Hoiem and R. Fergus. Indoor segmentation and support inference from RGBD images. In *ECCV*, 2012. 1, 2, 6, 7, 8
- [59] R. A. Newcombe, S. Izadi, O. Hilliges, D. Molyneaux, D. Kim, A. J. Davison, P. Kohi, J. Shotton, S. Hodges, and A. Fitzgibbon. KinectFusion: Real-time dense surface mapping and tracking. In *Mixed and augmented reality (ISMAR), 2011 10th IEEE international symposium on*, pages 127–136. IEEE, 2011. 2, 4

- [60] D. T. Nguyen, B.-S. Hua, L.-F. Yu, and S.-K. Yeung. A robust 3D-2D interactive tool for scene segmentation and annotation. *arXiv preprint arXiv:1610.05883*, 2016. 2, 3
- [61] B. Ni, G. Wang, and P. Moulin. RGBD-HuDaAct: A color-depth video database for human daily activity recognition. In *Consumer Depth Cameras for Computer Vision*, pages 193–208. Springer, 2013. 2
- [62] M. Nießner, M. Zollhöfer, S. Izadi, and M. Stamminger. Real-time 3D reconstruction at scale using voxel hashing. *ACM Transactions on Graphics (TOG)*, 32(6):169, 2013. 2, 4
- [63] Occipital. Occipital: The structure sensor, 2016. 3
- [64] K. Phillip and V. Koltun. Efficient inference in fully connected crfs with gaussian edge potentials. *Adv. Neural Inf. Process. Syst.*, 2011. 7
- [65] F. Pomerleau, S. Magnenat, F. Colas, M. Liu, and R. Siegwart. Tracking a depth camera: Parameter exploration for fast ICP. In *2011 IEEE/RSJ International Conference on Intelligent Robots and Systems*, pages 3824–3829. IEEE, 2011. 2
- [66] C. R. Qi, H. Su, M. Niessner, A. Dai, M. Yan, and L. J. Guibas. Volumetric and multi-view CNNs for object classification on 3D data. *arXiv preprint arXiv:1604.03265*, 2016. 2, 6, 8
- [67] X. Ren, L. Bo, and D. Fox. RGB-(D) scene labeling: Features and algorithms. In *Computer Vision and Pattern Recognition (CVPR), 2012 IEEE Conference on*, pages 2759–2766. IEEE, 2012. 2
- [68] A. Richtsfeld, T. Mörwald, J. Prankl, M. Zillich, and M. Vincze. Segmentation of unknown objects in indoor environments. In *2012 IEEE/RSJ International Conference on Intelligent Robots and Systems*, pages 4791–4796. IEEE, 2012. 2
- [69] B. C. Russell, A. Torralba, K. P. Murphy, and W. T. Freeman. LabelMe: a database and web-based tool for image annotation. *International journal of computer vision*, 77(1-3):157–173, 2008. 2
- [70] M. Savva, A. X. Chang, P. Hanrahan, M. Fisher, and M. Nießner. SceneGrok: Inferring action maps in 3D environments. *ACM Transactions on Graphics (TOG)*, 33(6):212, 2014. 2
- [71] M. Savva, A. X. Chang, P. Hanrahan, M. Fisher, and M. Nießner. PiGraphs: Learning interaction snapshots from observations. *ACM Transactions on Graphics (TOG)*, 35(4), 2016. 1, 2, 3
- [72] J. Shotton, B. Glocker, C. Zach, S. Izadi, A. Criminisi, and A. Fitzgibbon. Scene coordinate regression forests for camera relocalization in RGB-D images. In *Proceedings of the IEEE Conference on Computer Vision and Pattern Recognition*, pages 2930–2937, 2013. 2
- [73] A. Shrivastava and A. Gupta. Building part-based object detectors via 3D geometry. In *Proceedings of the IEEE International Conference on Computer Vision*, pages 1745–1752, 2013. 2
- [74] N. Silberman and R. Fergus. Indoor scene segmentation using a structured light sensor. In *Proceedings of the International Conference on Computer Vision - Workshop on 3D Representation and Recognition*, 2011. 1, 2
- [75] S. Song, S. P. Lichtenberg, and J. Xiao. SUN RGB-D: A RGB-D scene understanding benchmark suite. In *Proceedings of the IEEE Conference on Computer Vision and Pattern Recognition*, pages 567–576, 2015. 1, 2
- [76] S. Song and J. Xiao. Sliding shapes for 3D object detection in depth images. In *European Conference on Computer Vision*, pages 634–651. Springer, 2014. 2
- [77] S. Song and J. Xiao. Deep sliding shapes for amodal 3D object detection in RGB-D images. *arXiv preprint arXiv:1511.02300*, 2015. 1, 2
- [78] S. Song, F. Yu, A. Zeng, A. X. Chang, M. Savva, and T. Funkhouser. Semantic scene completion from a single depth image. *arXiv preprint arXiv:1611.08974*, 2016. 2
- [79] L. Spinello and K. O. Arras. People detection in RGB-D data. In *2011 IEEE/RSJ International Conference on Intelligent Robots and Systems*, pages 3838–3843. IEEE, 2011. 2
- [80] S. Stein and S. J. McKenna. Combining embedded accelerometers with computer vision for recognizing food preparation activities. In *Proceedings of the 2013 ACM international joint conference on Pervasive and ubiquitous computing*, pages 729–738. ACM, 2013. 2
- [81] J. Sturm, N. Engelhard, F. Endres, W. Burgard, and D. Cremers. A benchmark for the evaluation of RGB-D SLAM systems. In *2012 IEEE/RSJ International Conference on Intelligent Robots and Systems*, pages 573–580. IEEE, 2012. 1, 2
- [82] H. Su, S. Maji, E. Kalogerakis, and E. G. Learned-Miller. Multi-view convolutional neural networks for 3D shape recognition. In *Proc. ICCV*, 2015. 6
- [83] J. Sung, C. Ponce, B. Selman, and A. Saxena. Human activity detection from RGBD images. *plan, activity, and intent recognition*, 64, 2011. 2
- [84] A. Teichman, S. Miller, and S. Thrun. Unsupervised intrinsic calibration of depth sensors via SLAM. In *Robotics: Science and Systems*, volume 248, 2013. 3
- [85] J. Valentin, A. Dai, M. Nießner, P. Kohli, P. Torr, S. Izadi, and C. Keskin. Learning to navigate the energy landscape. *arXiv preprint arXiv:1603.05772*, 2016. 2
- [86] J. Valentin, V. Vineet, M.-M. Cheng, D. Kim, J. Shotton, P. Kohli, M. Nießner, A. Criminisi, S. Izadi, and P. Torr. SemanticPaint: Interactive 3D labeling and learning at your fingertips. *ACM Transactions on Graphics (TOG)*, 34(5):154, 2015. 2, 7
- [87] H. Wang, J. Wang, and W. Liang. Online reconstruction of indoor scenes from RGB-D streams. In *Proceedings of the IEEE Conference on Computer Vision and Pattern Recognition*, pages 3271–3279, 2016. 3
- [88] T. Whelan, M. Kaess, M. Fallon, H. Johannsson, J. Leonard, and J. McDonald. Kintinuous: Spatially extended KinectFusion. 2012. 4
- [89] T. Whelan, S. Leutenegger, R. F. Salas-Moreno, B. Glocker, and A. J. Davison. ElasticFusion: Dense SLAM without a pose graph. *Proc. Robotics: Science and Systems, Rome, Italy*, 2015. 4
- [90] T. Whelan, R. F. Salas-Moreno, B. Glocker, A. J. Davison, and S. Leutenegger. ElasticFusion: Real-time dense SLAM

- and light source estimation. *The International Journal of Robotics Research*, page 0278364916669237, 2016. [4](#)
- [91] Z. Wu, S. Song, A. Khosla, F. Yu, L. Zhang, X. Tang, and J. Xiao. 3D ShapeNets: A deep representation for volumetric shapes. In *Proceedings of the IEEE Conference on Computer Vision and Pattern Recognition*, pages 1912–1920, 2015. [1](#), [2](#), [6](#), [8](#)
 - [92] J. Xiao, A. Owens, and A. Torralba. SUN3D: A database of big spaces reconstructed using sfm and object labels. In *Computer Vision (ICCV), 2013 IEEE International Conference on*, pages 1625–1632. IEEE, 2013. [1](#), [2](#)
 - [93] B. Zeisl, K. Koser, and M. Pollefeys. Automatic registration of RGB-D scans via salient directions. In *Proceedings of the IEEE international conference on computer vision*, pages 2808–2815, 2013. [2](#)
 - [94] J. Zhang, C. Kan, A. G. Schwing, and R. Urtasun. Estimating the 3D layout of indoor scenes and its clutter from depth sensors. In *Proceedings of the IEEE International Conference on Computer Vision*, pages 1273–1280, 2013. [2](#)
 - [95] M. Zollhöfer, A. Dai, M. Innmann, C. Wu, M. Stamminger, C. Theobalt, and M. Nießner. Shading-based refinement on volumetric signed distance functions. *ACM Transactions on Graphics (TOG)*, 34(4):96, 2015. [2](#)